Cell Reports, Volume *38*

Supplemental information

Cross-species tropism and antigenic landscapes of circulating SARS-CoV-2 variants

Yali Zhang, Min Wei, Yangtao Wu, Juan Wang, Yuting Hong, Yang Huang, Lunzhi Yuan, Jian Ma, Kai Wang, Shaojuan Wang, Yang Shi, Zikang Wang, Huilin Guo, Jin Xiao, Chuanlai Yang, Jianghui Ye, Jijing Chen, Yuxi Liu, Baorong Fu, Miaolin Lan, Peixuan Gong, Zehong Huang, Yingying Su, Yixin Chen, Tianying Zhang, Jun Zhang, Huachen Zhu, Hai Yu, Quan Yuan, Tong Cheng, Yi Guan, and Ningshao Xia

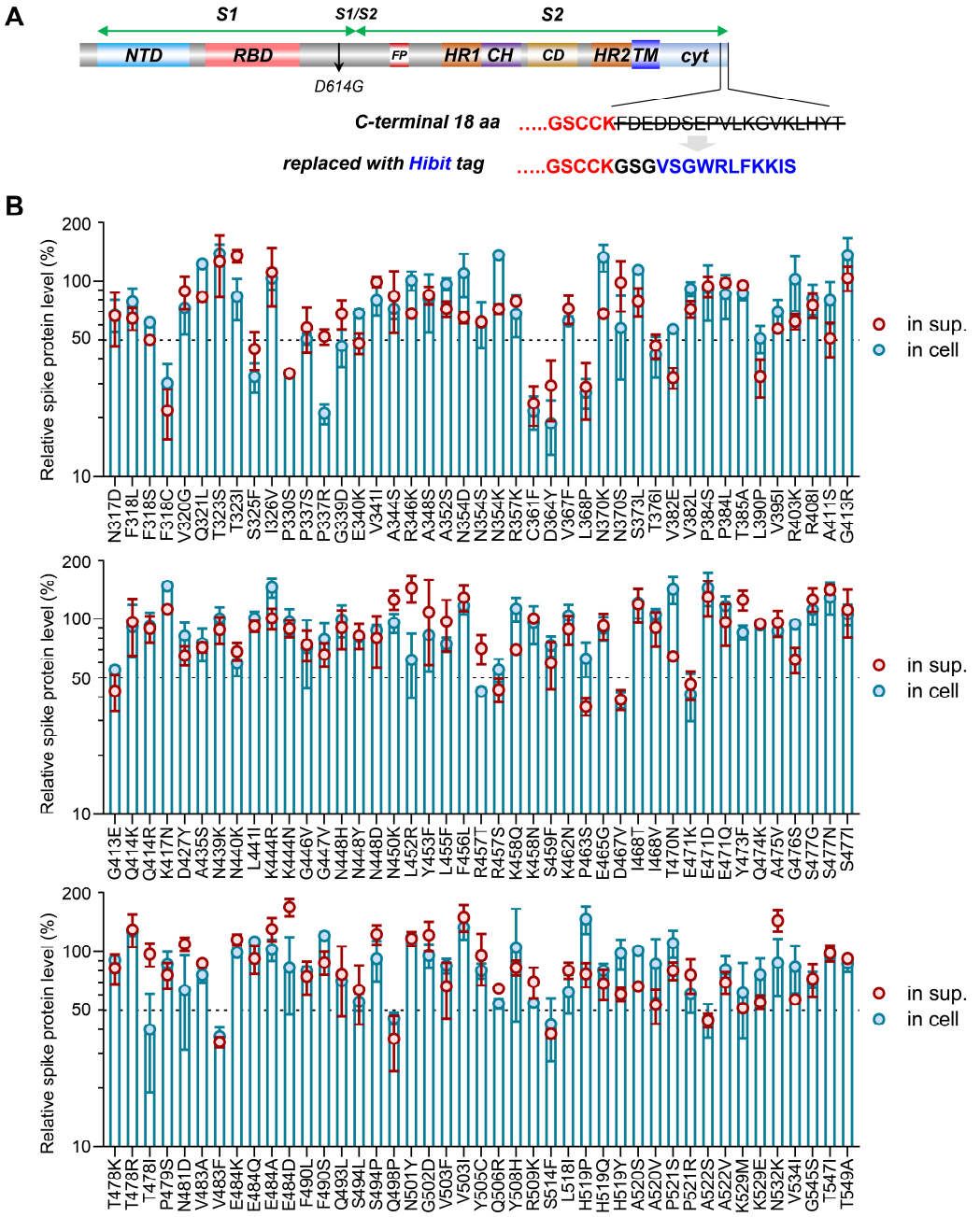

Figure S1. The productions and secretions of RBD mutants in 293T cells. Related to Figure 1. (A) Schematics of the spike variant-expressing cassette used in this study. The 18aa from the C-terminus of the spike was replaced with a HiBit bioluminescent tag for detection. **(B)** Changes of RBD mutants in spike production and secretion relative to S-614G control (%) in 293T cells. Extracellular and intracellular spike protein levels were detected by using Nano-Glo® HiBiT luminescent detection system. For each mutant, three technical replicates were performed. Data are plotted as the mean±SD. In sup. spike

protein level relative to S-614G in supernatants; in cell, spike protein level relative to S-614G in cell lysates. Seventeen mutants (F318C, S325F, P330S, P337R, G339D, C361F, D364Y, L368P, T376I, R457T, D467V, E471K, T478I, V483F, Q498P, S514F, A322S) present averagely >50% decreased spike-production (according to the relative spike levels in cell lysates). Seven mutants (N354D, N354K, N370K, K444R, K458Q, T470N, H519P) have notably decreased spike secretions (d-value between cell lysates and supernatants >40%).

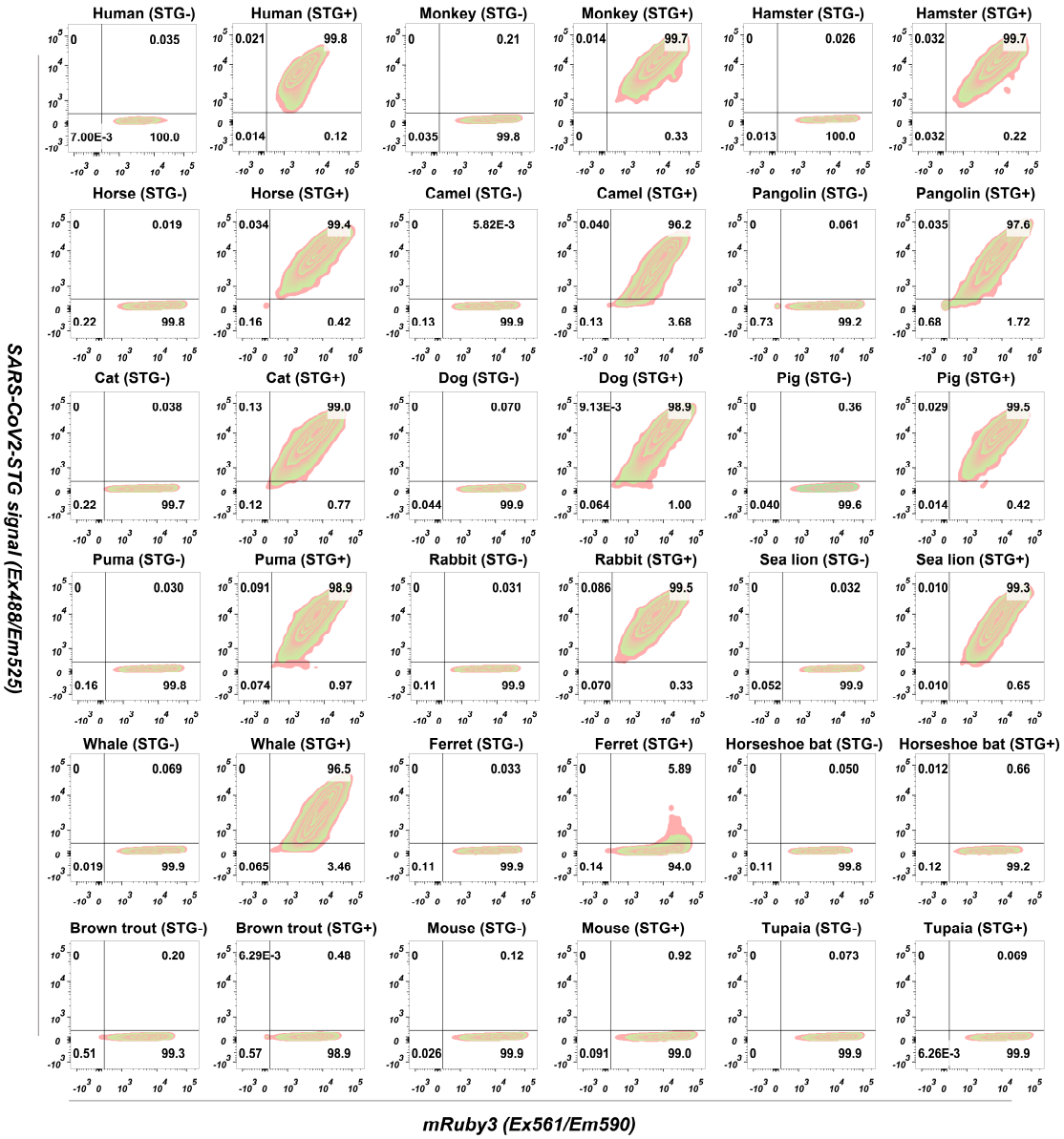

Figure S2. Flow cytometry analyses of H1299 cells expressing ACE2 orthologs of 18 species. Related to Figures 1 and 2. STG+, ACE2-expressing cells were pre-incubated (1 hour) with SARS-CoV2-STG probe; STG-, ACE2-expressing cells in the absence of SARS-CoV2-STG probe.

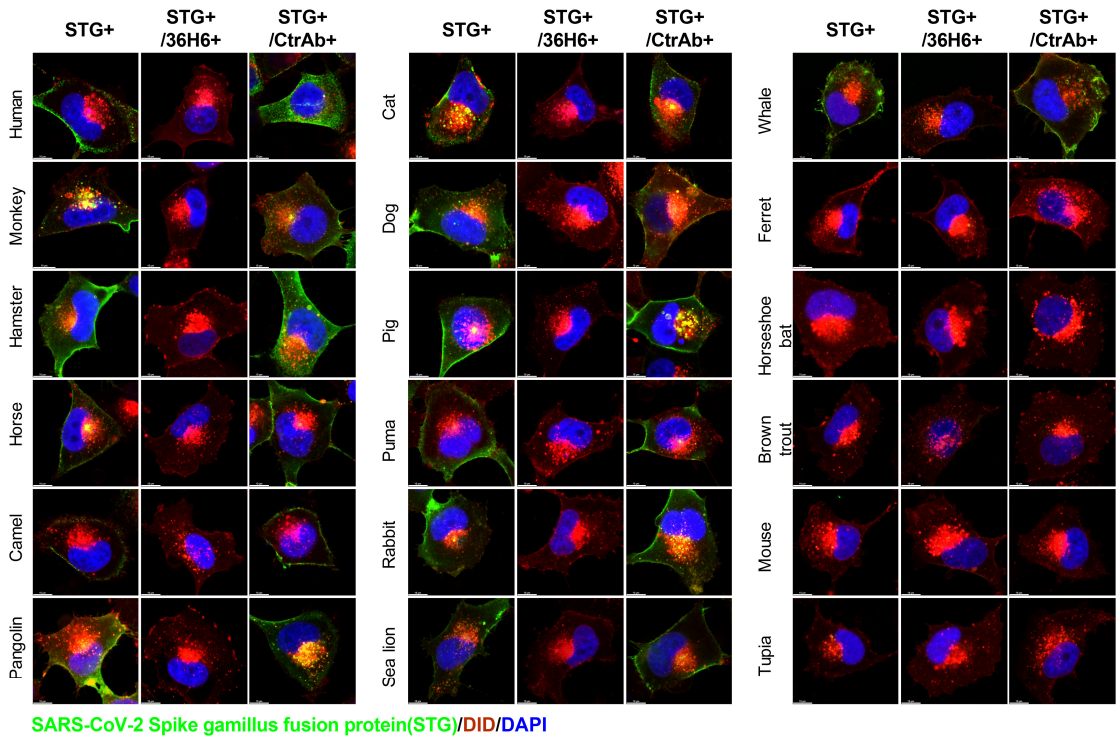

Figure S3. Fluorescence confocal images of ACE2-expressing cells incubated with SARS-CoV2-STG probe. Related to Figures 1 and 2. The SARS-CoV2-STG probe was used at 2.5 nM. STG+, cells were incubated (1 hour) with SARS-CoV2-STG probe; STG+/36H6+, cells were incubated with SARS-CoV2-STG in the presence of 36H6 mAb (a mAb can block the interaction between RBD and ACE2). STG+/CtrAb+, cells were incubated with SARS-CoV2-STG in the presence of a control mAb. DID, Membrane labeling DiD dye; DAPI, 4′,6-diamidino-2-phenylindole, DNA stain. The scale bar is 10 μm.

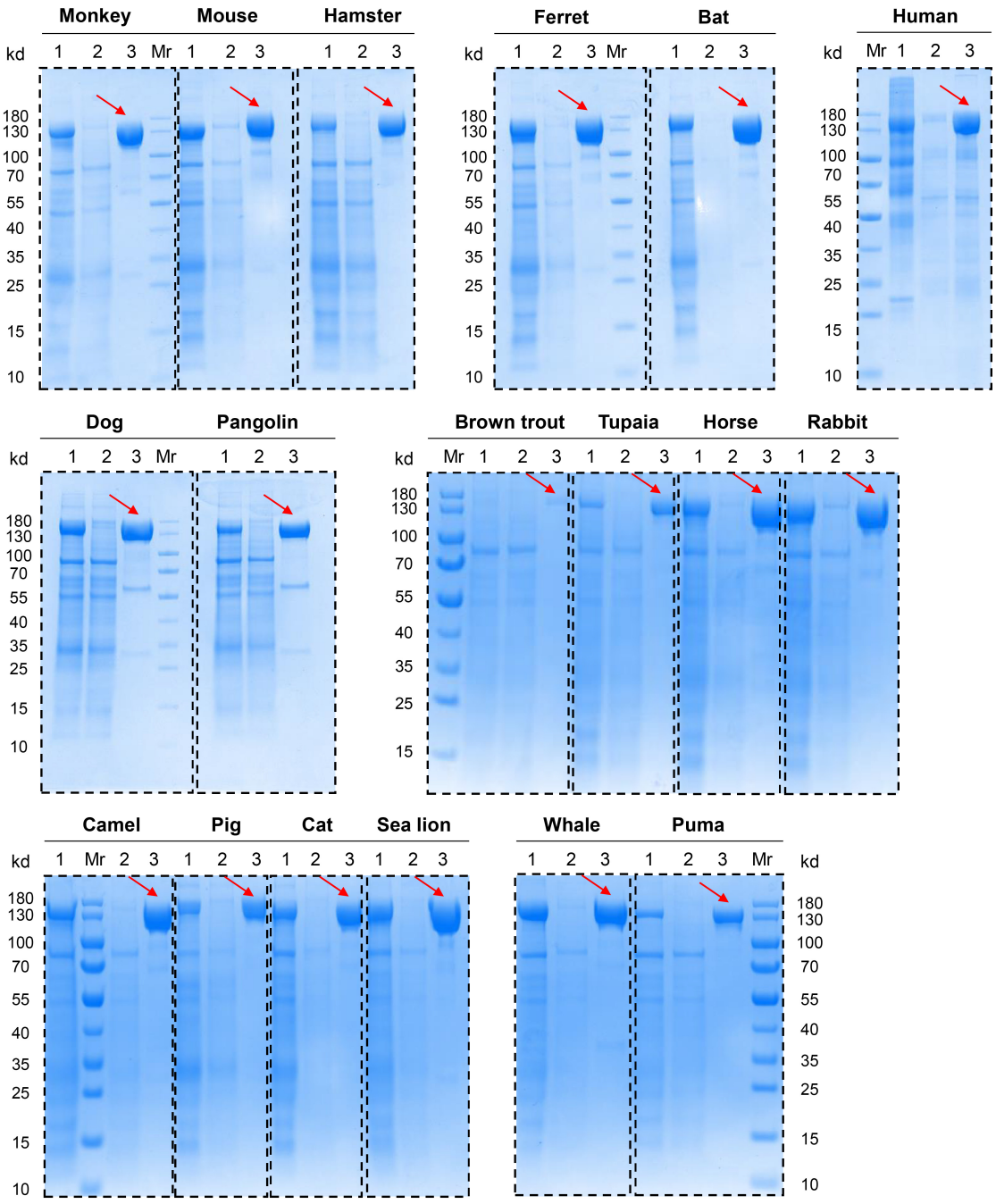

Figure S4. SDS-PAGE analyses of rACE2 proteins of various species. Related to Figures 1 and 3. lane 1, supernatants of transfected cells; lane 2, supernatants after flowing through MabSelect SuRe resin; lane 3, citrate buffer-eluted proteins; Mr, protein markers.

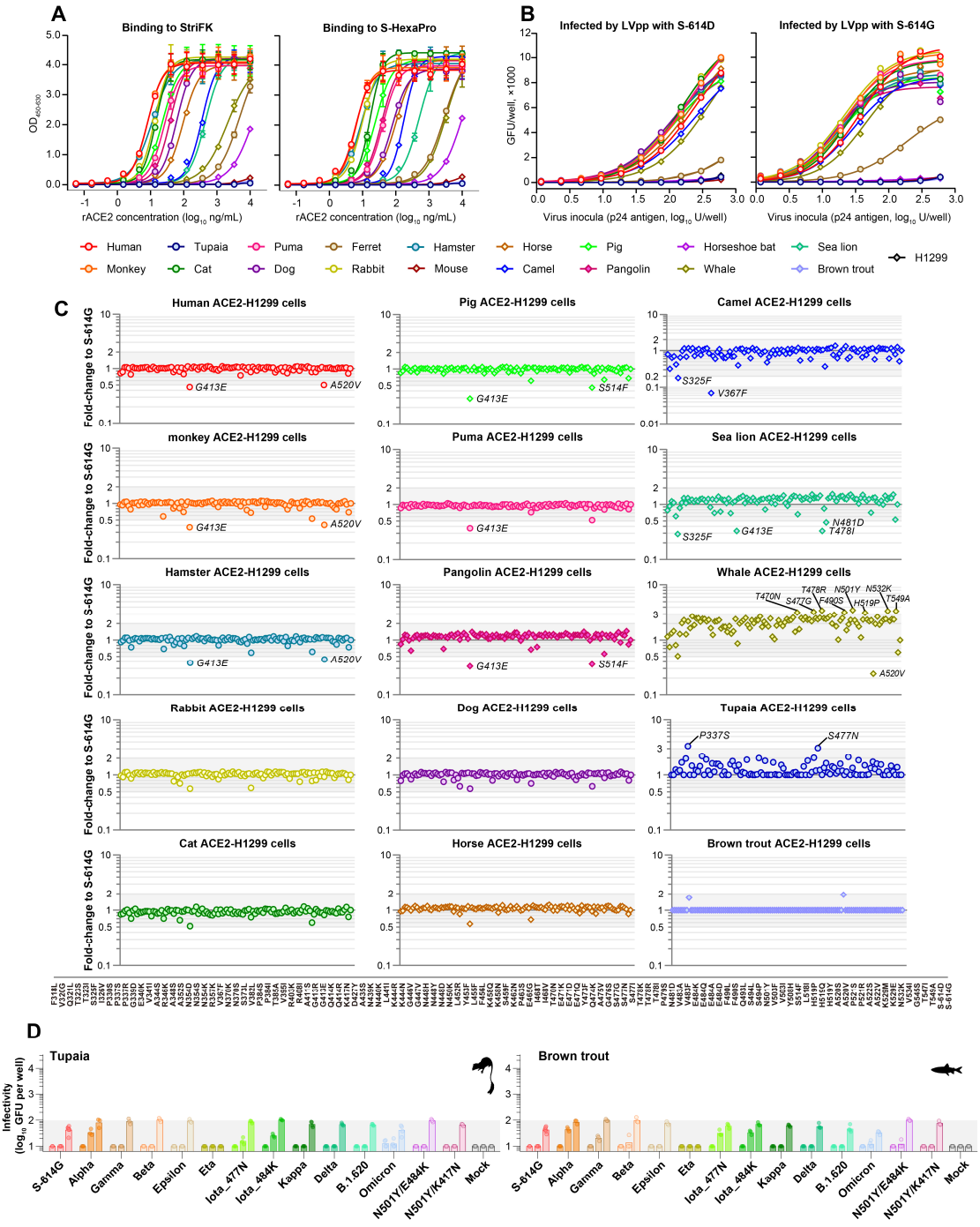

Figure S5. Evaluations on the spike-ACE2 ELISA binding and the infection performance of SARS-CoV-2 pseudovirus in ACE2-expressing cells. Related to Figures 1 and 2. (A) ELISA-binding activities of rACE2 proteins to immobilized StriFK (left panel) and S-HexaPro (right panel) proteins. Related to the left panel of Figure 1D. **(B)** Dose-dependent infection of S-614D (left panel) and S-614G (right panel) pseudovirus in H1299 cells expressing ACE2 orthologs of 18 species. Related to the right panel of Figure 1D. **(C)** The relative infection performance (fold change relative to the parental S-614G) of

RBD mutants in cells expressing 15 ACE2 orthologs, related to Figure 2A. **(D)** Comparison of the infectivities of VOC/VOI LVpp in cells expressing ACE2 orthologs of tupaia (left panel) or brown trout (right panel). Related to Figure 2C. Although some significant differences were noted for some variants in the two cells, markedly improved infection performance of variants was observed in neither tuACE2- nor btACE2-H1299 cells, suggesting the two ACE2 orthologs were still ineffective to support infection of these variants.

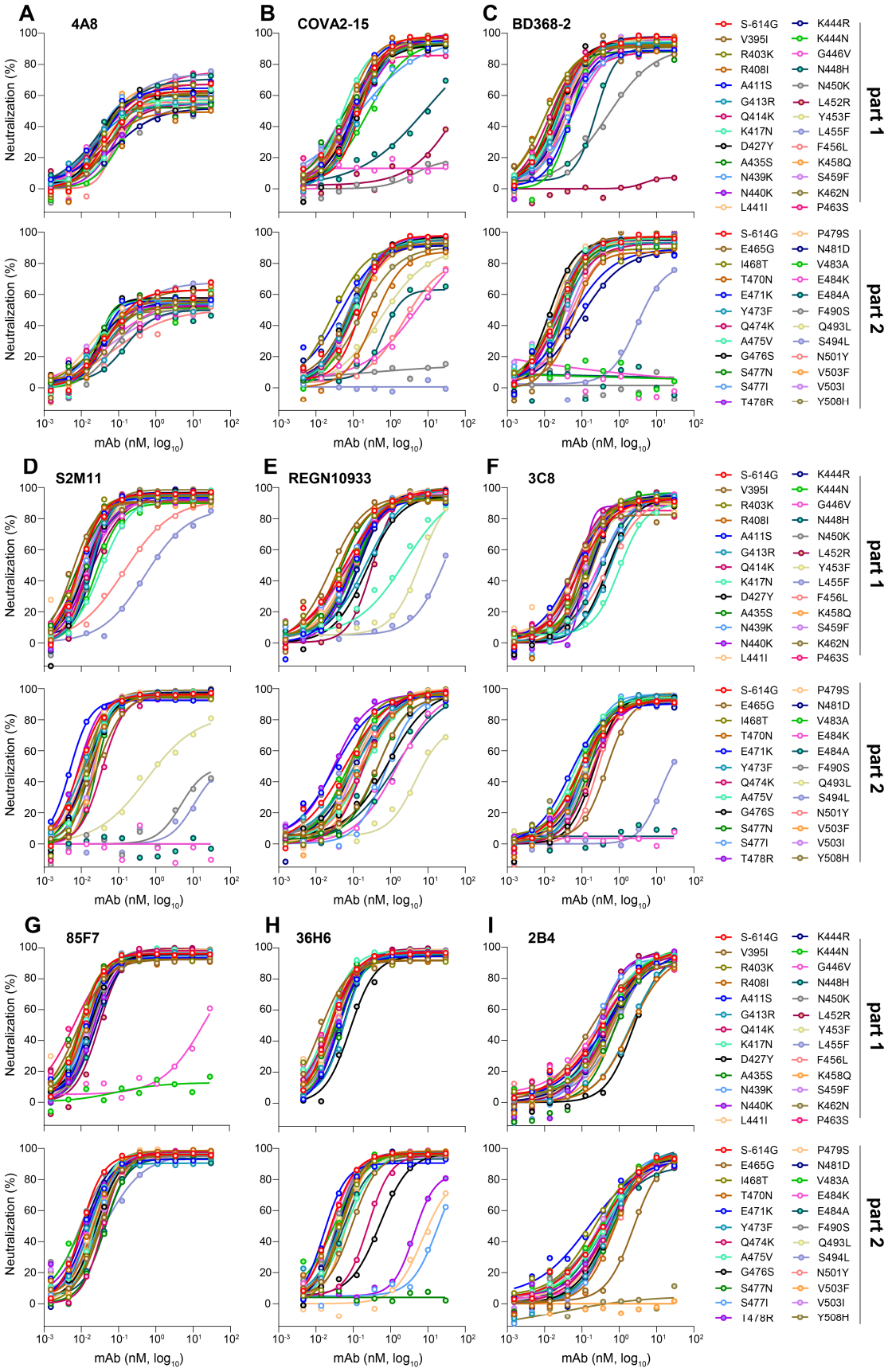

Figure S6. Neutralization profiles for 9 mAbs against 48 LVpp with single-site RBM mutation. Related to Figure 3. (A) human NTD mAb of 4A8; human RBD mAbs of

COVA2-15 **(B)**, BD368-2 **(C)**, S2M11 **(D)**, and REGN10933 **(E)**; mouse RBD mAbs of 3C8 **(F)**, 85F7 **(G)**, 36H6 **(H)**, and **(I)** 2B4. All mAbs were tested at 3-fold serial dilutions, related to Figure 3A.

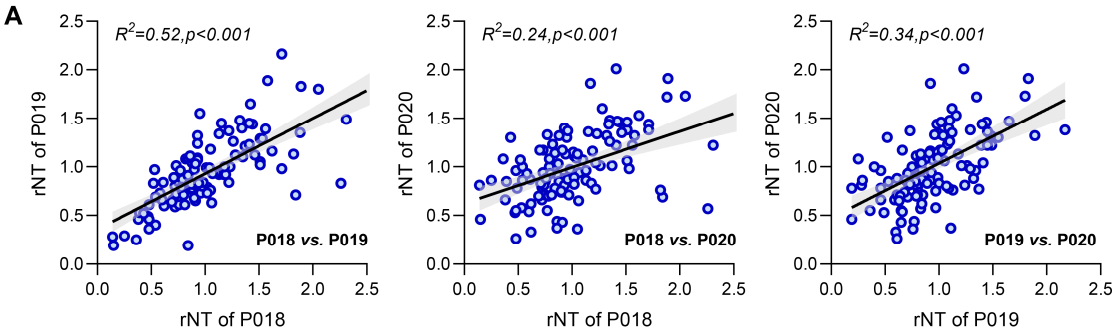

B

	Gender	Age	Disease	Sampled day	RBD mutations		S-614G	S-614D	Alpha	Gamma	Beta	Epsilon	Eta	Iota_477N	Iota_484K	Kappa	Delta	B.1.620	Omicron	SARS1rbd
										K417T	K417N								G339D K417N N440K S477N T478K E484A N501Y and other 9 mutations	
												L452R		S477N		L452R	L452R T478K	S477N		
									N501Y	E484K N501Y	E484K N501Y		E484K		E484K	E484Q		E484K		
P018	M	52	ns	45		NT, ID50	2553	1809	916	840	493	1983	1400	2334	2114	2717	1517	1437	5	190
						rNT	1.00	0.71	0.36	0.33	0.19	0.78	0.55	0.91	0.83	1.06	0.59	0.56	0.00	0.07
P019	F	57	s	60		NT, ID50	1929	1387	829	696	694	1695	1341	1501	1627	1024	1166	1041	5	133
						rNT	1.00	0.72	0.43	0.36	0.36	0.88	0.70	0.78	0.84	0.53	0.60	0.54	0.00	0.07
P020	M	33	ns	39		NT, ID50	2541	2209	1157	229	174	836	690	2626	1245	632	1097	717	26	308
						rNT	1.00	0.87	0.46	0.09	0.07	0.33	0.27	1.03	0.49	0.25	0.43	0.28	0.01	0.12

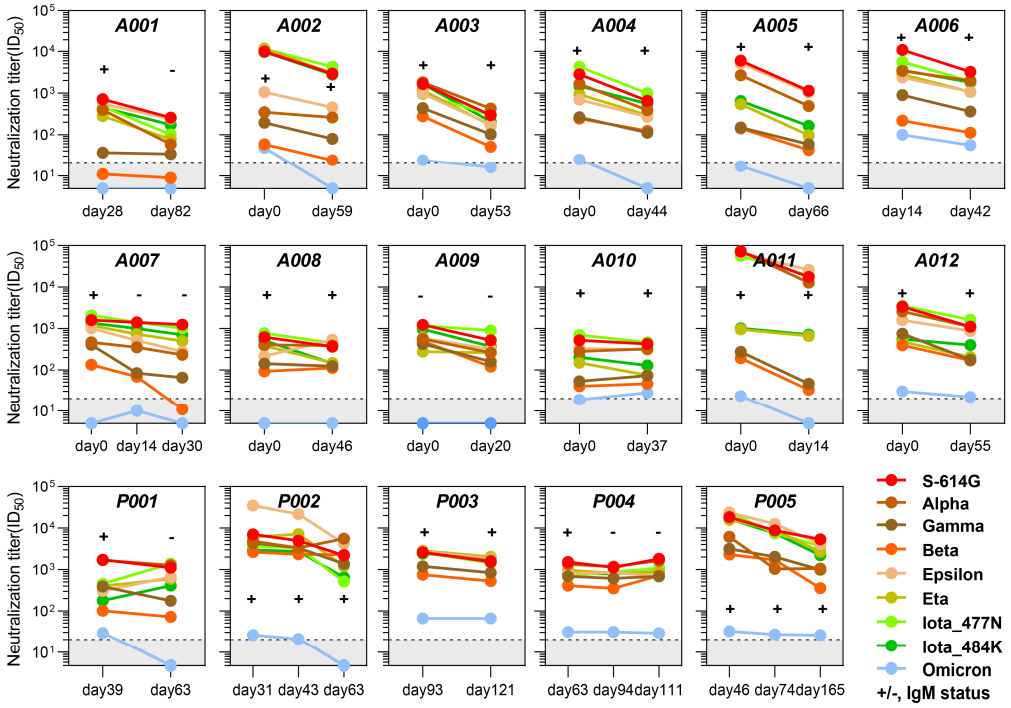

Figure S7. Multiplexed analysis of HCPs against variants. Related to Figure 3. (A) Correlation analyses of the rNT against 112 single-site RBD mutants of P018 *v.s* P019, P018 *v.s* P020, and P019 *vs.* P020. **(B)** The cross-neutralizing profiles of P018, P019, and P020 against the VOC/VOI variants. The NT data are ID50. The rNT= the ratio of NT against variant/NT against S-614G. The color changes from red to blue indicate the decreasing rNT. RBD mutations of the VOC/VOI variants are shown in the table. All the 3 HCPs were from the patient group. 'Disease' indicated the COVID-19 severity. S, severe;

ns, non-severe. 'Sampled day' indicated the sampling day since disease onset. SARS1rbd, pseudovirus bearing a chimeric spike of SARS-CoV-2 with SARS-CoV RBD replacement. **(C)** Longitudinal cross-neutralization profiles of HCPs from individuals (ASI) with past asymptomatic (n=12, A001 to A012) or symptomatic (n=5, P001 to P005) infections. The time points of samples are days since SARS-CoV-2 antibody seroconversion for ASIs and are days since illness onset for patients.

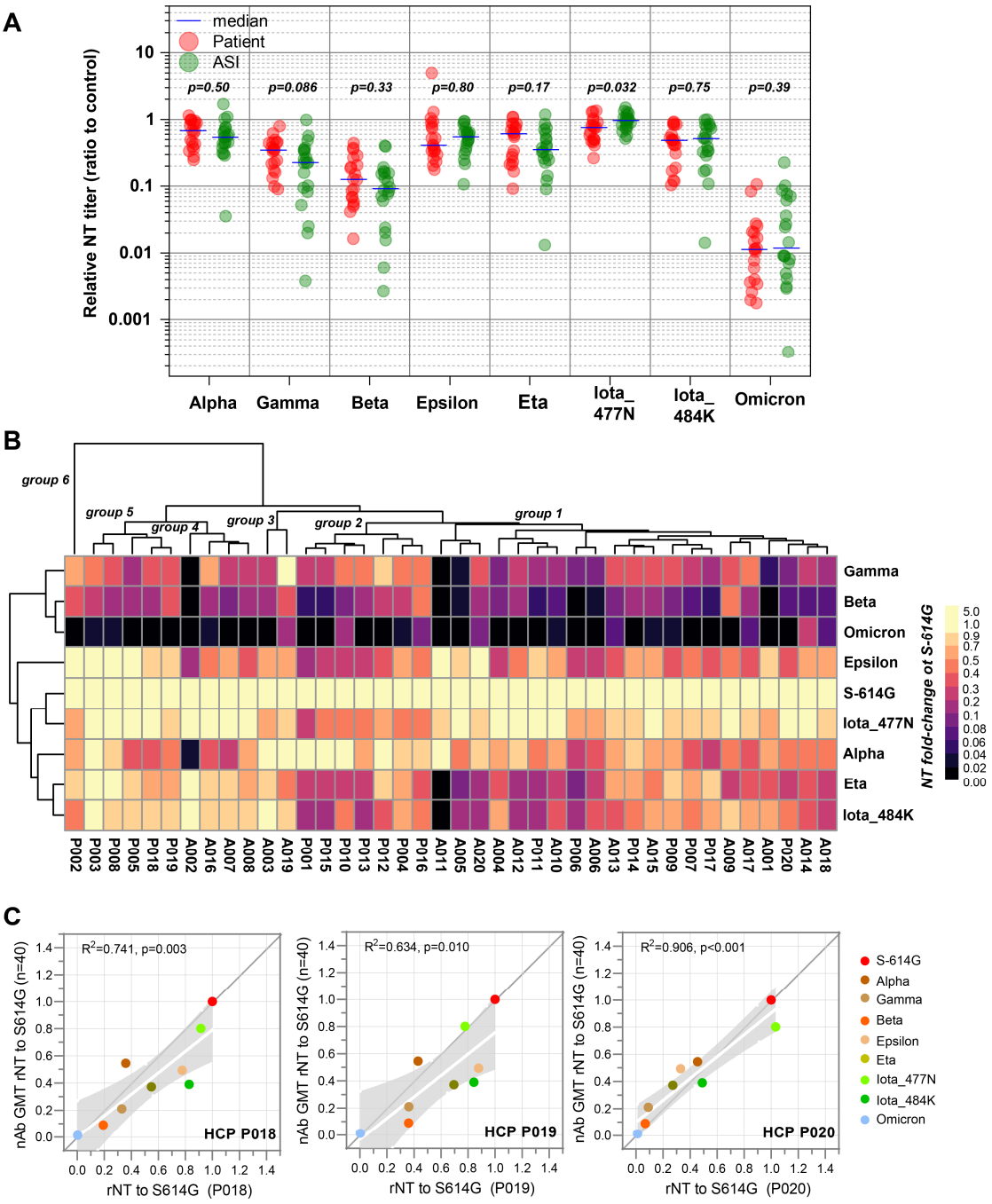

Figure S8. Grouping HCPs by cross-neutralization patterns. Related to Figure 3. (A) Comparisons of the rNT against VOC/VOI variants between HCPs from patients and ASI cases. **(B)** Classification of HCP samples according to their cross-neutralization profiles against VOC/VOI variants. A heatmap representation of cross-neutralization profiles of HCPs was generated based on the rNT of the sample against each variant. The groups (groups 1 to 6) of HCPs are divided by hierarchical clustering. **(C)** Correlation analyses of the cross-variants rNT of the three representative HCPs and the average level (GMT) of the total HCP cohort (n=40).

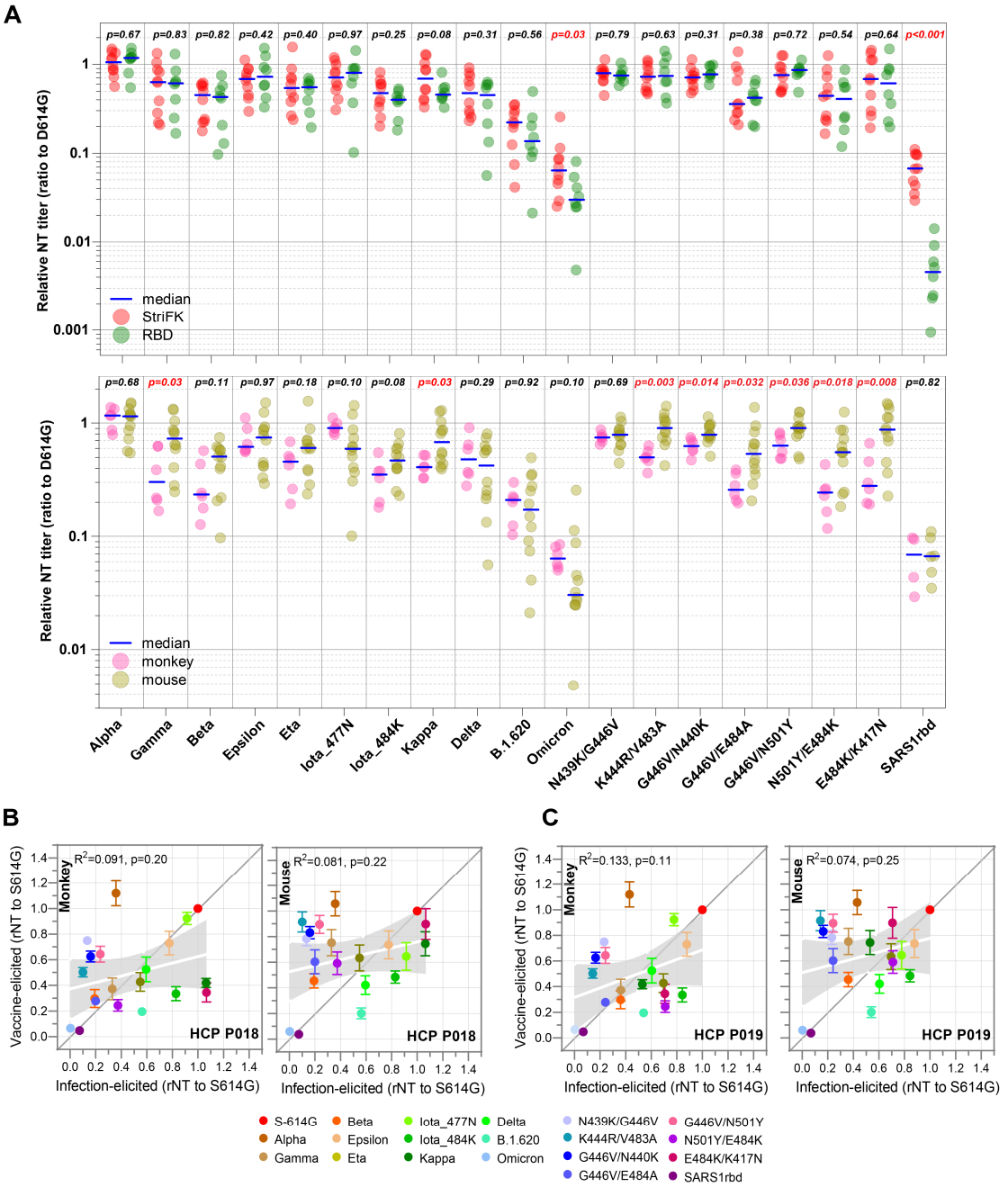

Figure S9. Comparisons of the cross-neutralization breadth of antisera of animals received protein-based vaccines. Related to Figure 4. (A) Difference of the rNT against variants of antisera from recombinant spike or RBD protein-based vaccine (3-shot) immunized monkeys and mice. The upper panel shows the comparison between recombinant StriFK (n=10) and RBD (n=8) vaccinated animals (pooled monkeys and mice). The lower panel shows the comparison between monkeys (n=6) and mice (n=12). For the SARS1rbd group of the lower panel, due to the significant difference between StriFK and RBD groups, only the data of the StriFK group are included for inter-animal comparison (4

monkeys *v.s.* 6 mice). Unpaired t-test or Mann-Whitney U test was used to compare continuous variables between two groups according to the data distribution. Comparison of the rNT of HCP P018 **(B)** or P019 **(C)** (X-axis) and spike-based vaccine-elicited animal's sera (Y-axis; left panel, in monkeys; right panel, in mice) against SARS-CoV-2 variants**.** For both panels **(B)** and **(C)**, the data are plotted as mean±SEM.

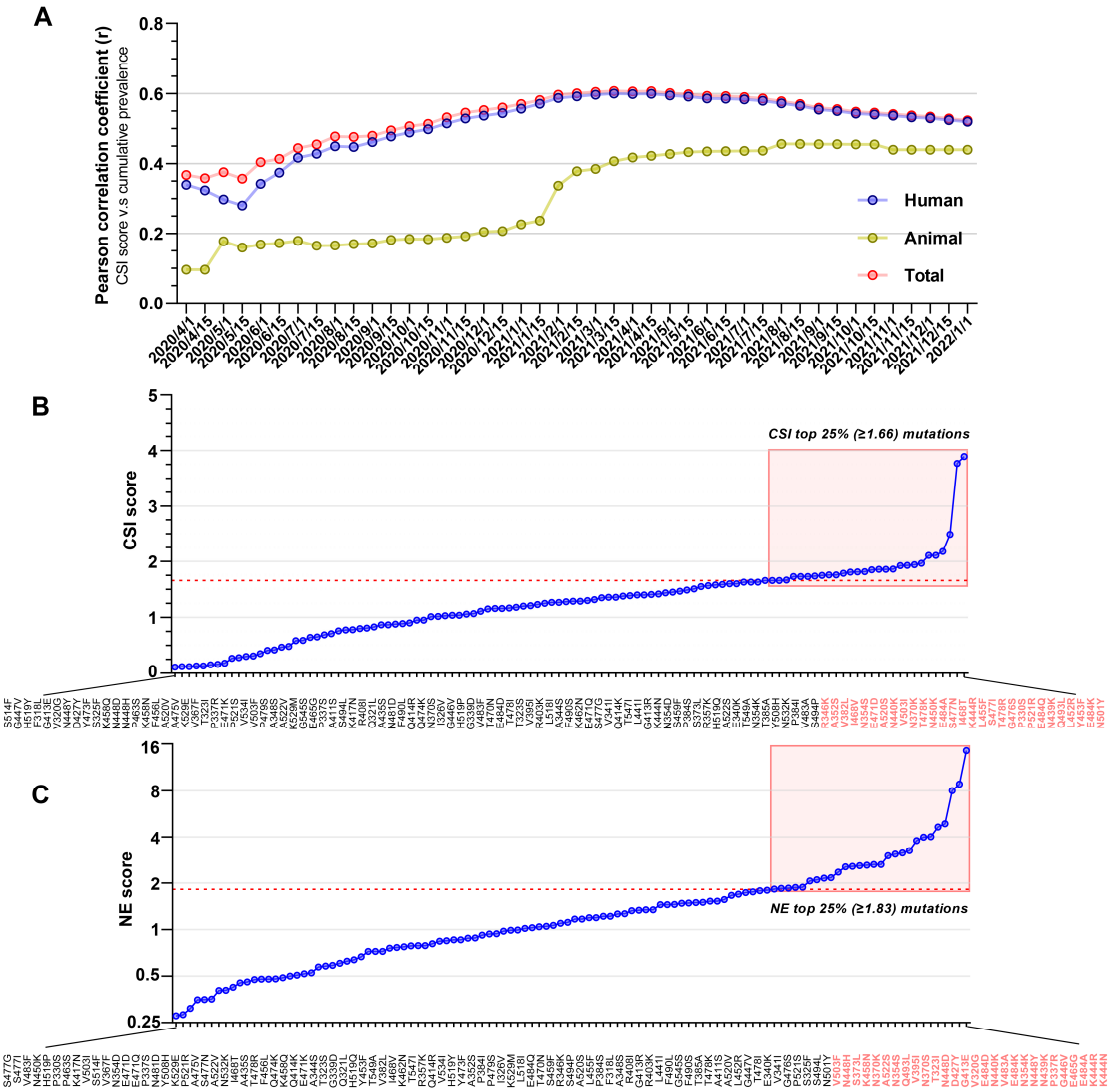

Figure S10. The CSI and NE scores of RBD mutations. Related to Figure 5. (A) Dynamics of the Pearson correlation coefficient (r) between the CSI score and the cumulative prevalence of mutations in human-derived, non-human animal-derived, and total viral sequences in GISAID during the pandemic. Ranking of the CSI **(B)** and NE **(C)** scores of 112 RBD mutations. Following the statistical distributions of the two scores, the 75% percentile is 1.66 for the CSI score and is 1.83 for the NE score. Mutations with the top 25% CSI (≥1.66, n=29) or NE scores (≥1.83, n=28) are highlighted with red frames.

Table S1. Information of the ACE2 orthologs of various animals involved in the study. Related to Figure 1.

Species	Abbreviation	Sequence ID
Homo sapiens	Human	NM_021804.3
Macaca mulatta	Monkey	XM_028841825.1
Tupaia chinensis	Tupaia	XM_006164692.3
Felis catus	Cat	NM_001039456.1
Puma concolor	Puma	XM_025934632
Canis lupus familiaris	Dog	NM_001165260.1
Mustela putorius furo	Ferret	XM_004758886.2
Oryctolagus cuniculus	Rabbit	XM_002719845.3
Mesocricetus auratus	Hamster	XM_005074209.2
Mus musculus	Mouse	NM_001130513.1
Equus przewalskii	Horse	XM_008544773.1
Camelus ferus	Camel	XM_006194201.2
Sus scrofa	Pig	XM_021079374.1
Manis javanica	Pangolin	XM_017650263.2
Rhinolophus ferrumequinum	Horseshoe bat	XM_033107295.1
Physeter catodon	Whale	XM_024115511.2
Eumetopias jubatus	Sea Lion	XM_028115021.1
Salmo trutta	Brown Trout	XM_029747397.1

Table S2. Characteristics of the convalescent individuals with COVID-19 disease or past asymptomatic infections (ASIs) involved in this study. Related to Figure 3.

		COVID-19 patients	Asymptomatic infections	Total
No.		20	20	40
Gender (M/F)		11/9	12/8	23/17
Age, median (range)		51 (30-68)	50 (30-58)	51 (30-68)
Sampled at day after onset [a]		39 (14-93)	NA	39 (14-93)
No. with severe-to-critical disease		4	0	4
No. with longitudinal samples		5	12	17
Days of follow-up, median (range)		32 (24-119)	45 (14-66)	44 (14-119)
RBD-IgM seropositivity, no.(%) [b]		15 (75%)	13 (65%)	28 (70%)
RBD-IgG seropositivity, no.(%) [b]		20 (100%)	20 (100%)	40 (100%)
NT to S-614G	Level, log_{10}	3.70±0.39	3.08±0.77	3.41±0.68
	Reference [c]	1.0	1.0	1.0
NT to Alpha	Level, log_{10}	3.54±0.34	2.64±0.82	3.24±0.71
	Fold change [d]	0.68 (0.25-1.14)	0.54 (0.035-1.70)	0.57 (0.035-1.70)
NT to Gamma	Level, log_{10}	3.16±0.36	2.23±0.55	2.74±0.65
	Fold change [d]	0.35 (0.09-0.80)	0.23 (0.004-0.97)	0.26 (0.004-0.97)
NT to Beta	Level, log_{10}	2.74±0.43	2.05±0.62	2.41±0.68
	Fold change [d]	0.13 (0.016-0.44)	0.09 (0.003-0.40)	0.11 (0.003-0.44)
NT to Epsilon	Level, log_{10}	3.35±0.54	2.80±0.78	3.03±0.74
	Fold change [d]	0.41 (0.18-4.95)	0.55 (0.11-0.94)	0.50 (0.11-4.95)
NT to Eta	Level, log_{10}	3.21±0.40	2.51±0.67	3.01±0.68
	Fold change [d]	0.61 (0.09-1.10)	0.35 (0.013-1.18)	0.40 (0.013-1.18)
NT to Iota_477N	Level, log_{10}	3.45±0.47	2.98±0.77	3.34±0.68
	Fold change [d]	0.75 (0.26-1.36)	0.96 (0.52-1.52)	0.82 (0.26-1.52)
NT to Iota_484K	Level, log_{10}	3.29±0.43	2.73±0.68	3.10±0.65
	Fold change [d]	0.49 (0.10-0.93)	0.51 (0.014-1.00)	0.49 (0.014-1.00)
NT to Omicron	Level, log_{10}	1.75±0.51	1.32±0.51	1.44±0.55
	Fold change [d]	0.01 (0.002-0.11)	0.01 (0.0003-0.23)	0.01 (0.0003-0.23)

[a] It is the first sampling time after illness onset. [b] Serological status of RBD-IgM/IgG for the 1st sample of each case. [c] The NT of each HCP sample against the S-614G is regarded as the reference. [d] Indicating the fold changes of NT to a variant in comparison with that to S-614G control. The data of NT level is expressed as median±SD. The fold-change of NT to VOCs is median (range).

Table S3. Multivariate analysis of the effects of RBD mutations for the cross-species breakout potentials and on the neutralization escape to representative HCPs in associating with their cumulative frequencies at different time points. Related to Figure 5.

	To cumulative frequencies of mutations, β (p value)		
	in humans	in animals	in total
By January 1, 2022			
rNT of HCP P018	-0.083 (0.79)	0.057 (0.80)	-0.054 (0.86)
rNT of HCP P019	0.328 (0.45)	-0.032 (0.92)	0.311 (0.48)
rNT of HCP P020	-0.253 (0.46)	-0.142 (0.56)	-0.267 (0.43)
Infectivity in huACE2 cells	-0.019 (0.94)	-0.193 (0.32)	-0.024 (0.93)
Infectivity in feACE2 cells	0.712 (0.0002)	0.540 (<0.0001)	0.721 (0.0001)
Infectivity in muACE2 cells	0.037 (0.0021)	0.021 (0.013)	0.037 (0.002)
By July 1, 2021			
rNT of HCP P018	-0.070 (0.80)	0.076 (0.72)	-0.007 (0.98)
rNT of HCP P019	0.241 (0.54)	-0.058 (0.84)	0.200 (0.60)
rNT of HCP P020	0.018 (0.95)	-0.082 (0.72)	-0.012 (0.97)
Infectivity in huACE2 cells	0.010 (0.97)	-0.254 (0.16)	0.004 (0.99)
Infectivity in feACE2 cells	0.737 (<0.0001)	0.510 (<0.0001)	0.751 (<0.0001)
Infectivity in muACE2 cells	0.043 (<0.0001)	0.022 (0.0064)	0.043 (<0.0001)
By January 1, 2021			
rNT of HCP P018	-0.089 (0.73)	0.032 (0.87)	-0.008 (0.97)
rNT of HCP P019	0.025 (0.94)	-0.025 (0.93)	-0.015 (0.97)
rNT of HCP P020	0.285 (0.31)	0.105 (0.64)	0.244 (0.37)
Infectivity in huACE2 cells	0.029 (0.89)	-0.284 (0.10)	0.031 (0.89)
Infectivity in feACE2 cells	0.697 (<0.0001)	0.424 (0.0005)	0.717 (<0.0001)
Infectivity in muACE2 cells	0.030 (0.002)	-0.008 (0.33)	0.030 (0.002)
By July 1, 2020			
rNT of HCP P018	-0.137 (0.53)	0.015 (0.92)	0.029 (0.89)
rNT of HCP P019	0.202 (0.51)	0.026 (0.90)	0.108 (0.70)
rNT of HCP P020	0.161 (0.50)	0.084 (0.60)	0.082 (0.71)
Infectivity in huACE2 cells	-0.179 (0.34)	-0.191 (0.13)	-0.163 (0.35)
Infectivity in feACE2 cells	0.493 (0.0002)	0.244 (0.005)	0.525 (<0.0001)
Infectivity in muACE2 cells	0.011 (0.18)	-0.004 (0.42)	0.010 (0.18)